

Optimum energy window setting on Hg-201 x-rays photopeak for effective Tl-201 imaging

Akihiro KOJIMA,* Akihiro TAKAKI,** Teruya NOGUCHI,*** Masanori MATSUMOTO,****
Noboru KATSUDA,***** Seiji TOMIGUCHI***** and Yasuyuki YAMASHITA*****

*Institute of Resource Development and Analysis, Kumamoto University

**Daiichi Radioisotope Laboratories

***Kumamoto Regional Medical Center

****Course of Radiological Sciences, Kumamoto University School of Health Sciences

*****Department of Radiology, Kumamoto University School of Medicine

For more effective Tl-201 imaging, the location and width of the energy window set on the Hg-201 x-rays photopeak was investigated using Monte Carlo simulation and phantom experiments. We calculated energy spectra and investigated the amount of primary and scattered photons within various energy windows set on the x-rays photopeak. The energy resolution (ER) at 71 keV (the peak of the x-rays photopeak) was changed to 10%, 12%, 14% and 16%. The relationships between the energy window and the primary counts rate or the scatter fraction (= scattered counts/primary counts, SF) were obtained. By compromise between the primary counts rate and the SF for ER = 12%, the optimum energy window was determined as a wider off-peak window, $77 \text{ keV} \pm 14.3\%$ (66–88 keV). This off-peak window increased the primary counts rate by 12.5% and decreased the SF by ~17% as compared with the conventional on-peak energy window ($71 \text{ keV} \pm 10\%$, 64–78 keV). When this off-peak widow acquisition was compared with the conventional on-peak window one on a gamma camera, planar and SPECT images using the off-peak widow clearly showed superior results qualitatively and quantitatively.

Key words: Tl-201 imaging, Hg-201 x-rays photopeak, off-peak energy window, Monte Carlo simulation, phantom experiment

INTRODUCTION

THALLIUM-201 (Tl-201) is one of the radionuclides used extensively in scintigraphic imaging of the heart,¹ thyroid,² tumor,³ and so on. Tl-201 has a physical half-life of 73.1 hr and decays by electron capture to mercury-201 (Hg-201). Although the multiple energy characteristic x-rays of Hg-201 (69–83 keV) and some gamma rays of Tl-201 (135 and 167 keV) are emitted,⁴ the Hg-201 x-rays are commonly used for imaging due to the low abundance of two gamma rays. When these x-rays are detected with a gamma camera, the shape of the x-rays photopeak is not

a simple Gaussian form with a shoulder at the upper part of the photopeak and a wide energetic spread due to a relatively poor energy resolution of gamma cameras. This shoulder has been observed on the energy spectrum of the newer gamma camera with the better energy resolution (<10% at 140 keV of technetium-99m).⁵ In general, data acquisition for Tl-201 imaging is performed with an energy window centered on the peak of the photopeak region at 71 keV.⁶

Due to the finite energy resolution of gamma cameras, scattered photons are inevitably detected with primary photons within the photopeak window. Scattered photons reduce cold-lesion contrast and blur edges of accumulated radionuclides, and furthermore, degrade quantification of radioactivity. Especially, inclusion of scatter greatly affects low-energy photons imaging together with attenuation in the body. Therefore, in order to reduce the contribution of scatter to a specified photopeak window in

Received December 6, 2004, revision accepted July 4, 2005.

For reprint contact: Akihiro Kojima, Ph.D., Institute of Resource, Development and Analysis, Kumamoto University, 2–2–1 Honjo, Kumamoto 860–0811, JAPAN.

E-mail: akojima@kaiju.medic.kumamoto-u.ac.jp

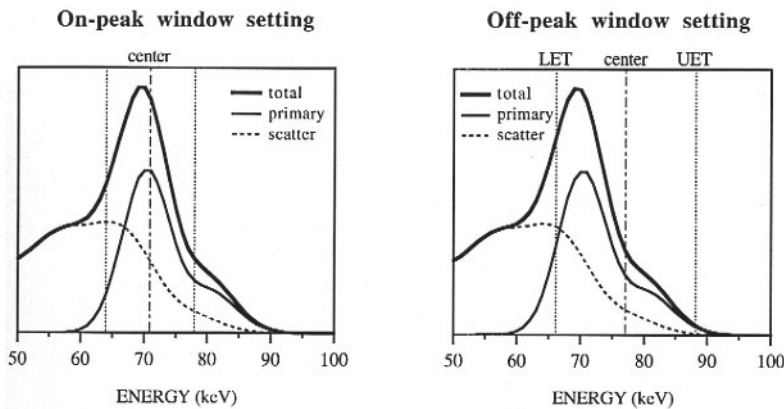


Fig. 1 Energy window setting for an on-peak window and an off-peak window on the photopeak region of the Hg-201 x-rays. For the on-peak window, its center was placed on the peak at 71 keV. For the off-peak window, the window center with the lower energy threshold (LET) and upper energy threshold (UET) was shifted toward the lower or higher energy side of the photopeak.

Tl-201 imaging, it is necessary to consider the energy window setting carefully.

The aim of this study was to determine the optimum energy window setting for various energy resolutions in Tl-201 imaging using Monte Carlo simulation and validate it on phantom experiments using the gamma camera. The “optimum energy window” means the window that can decrease the scattered photons relatively or reduce the scatter fraction (the ratio of scattered to primary photons, SF) while increasing the primary counts rate. In this study, the energy resolution was changed from 10% to 16% at 71 keV. For each energy resolution, the relationships between the primary counts and the energy window, and the SF and the energy window were obtained. For the Tl-201 imaging experiment, a plate phantom with multiple defects and a myocardial phantom were employed.

MATERIALS AND METHODS

Monte Carlo simulation

In this investigation, we performed the Monte Carlo simulation for Tl-201 imaging as we reported the energy spectrum calculations of Tl-201⁵ and Tc-99m.⁷

A Tl-201 line source of 5 cm was simulated within a water-filled tank (30 cm × 30 cm × 14 cm) with the 4 cm-forward scatter and the 10 cm-backscatter. The multiple x-rays with 69 (intensity of 26.9%), 71 (46.4%), 80 (16.1%), and 83 keV (4.4%) for Hg-201, and the gamma rays of 135 (2.67%) and 167 keV (9.4%) for Tl-201 were considered.⁴ The three photon-interactions, photoelectric effect, Compton, and coherent scattering, were simulated with scattering up to the order of six for all the x-rays and the order of nine for all the gamma rays. Thirteen million photons were generated from the line source. A parallel-hole collimator was simulated and all photons with incidental angles below 1° to the axis of the collimator hole were accepted. Then, the crystal energy efficiency was

assumed to be 100% for all energy ranges. The detected area on the collimator face was a region of interest (ROI) of 12 cm × 10 cm. No scatter from the collimator or crystal was considered.

We calculated the energy spectra for the line source as follows. First, the separated energy spectra corresponding to primary and scattered photons were calculated with an energy resolution of 1 keV full width at half maximum (FWHM). Second, to simulate the degraded energy spectra of practical gamma cameras, these ideal energy spectra were convolved with Gaussian functions corresponding to the finite energy resolution. Finally, the energy spectra for total events were obtained by summing primary and scattering counts. The energy resolution was changed to 10, 12, 14 and 16% at 71 keV.

The two ways of the energy window setting on the photopeak region of the multiple energy x-rays were considered: an on-peak window and an off-peak window (Fig. 1). For the on-peak window, whose center is set on the peak at 71 keV, its width was varied from 20% to 39%. In the off-peak window setting, the lower energy threshold was set at 63, 64, 65, 66, and 67 keV while the upper energy threshold was varied from 78 to 90 keV in 1 keV increments for each lower energy threshold.

The counts for both the primary and scattered photons within these energy windows were integrated and the scatter fraction (SF), defined as the ratio of scattered counts to primary counts, was calculated. Consequently, the relationships between the energy window and the relative primary counts (the ratio for the total primary counts of the photopeak) or the SF were obtained at various energy resolutions.

Phantom experiments

A dual-headed gamma camera equipped with two low-energy, general purpose (LEGP), parallel-hole collimators (GCA-7200A/DI, Toshiba, Japan) and a nuclear

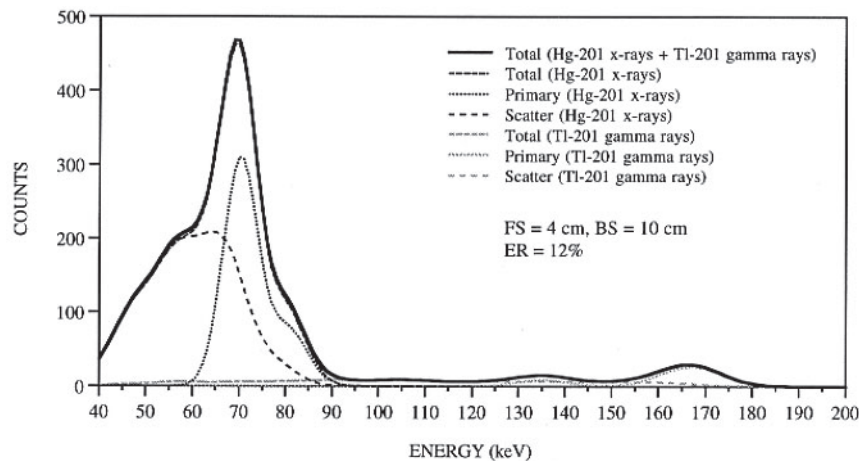


Fig. 2 Energy spectra simulated for a Tl-201 line source within scattering materials (water) with 4 cm-forward scatter (FS) and 10 cm-backscatter (BS). The energy resolution (ER) was 12%.

medicine computer system (GMS-5500/DI, Toshiba, Japan) were used for data acquisitions and processing. The energy resolution was 12% at 71 keV.⁵

A. Planar imaging

A Tl-201 line source of 5 cm (5.4 MBq) and a plate phantom (25.5 cm × 15.5 cm × 0.7 cm, Tl-201 of 38.9 MBq) with ten different-sized defects (0.5 cm ϕ –4.0 cm ϕ) were prepared. Both Tl-201 sources were placed at the 4 cm-forward scatter and the 10 cm-backscatter of water-equivalent materials (30 cm × 30 cm × 14 cm, Tough water phantom, Kyoto Kagaku, Japan). Planar images were acquired with 256 × 256 matrices, a zoom factor of 2.0, and a pixel size of 1.1 mm. The source-to-collimator distance was 12 cm and acquisition time was 10 min.

From the Tl-201 line source images, SF value, FWHM, and full width at tenth maximum (FWTM) were measured. The SF value was calculated in the following manner. Scatter count S(d) at thickness d is given by

$$S(d) = T(d) - P(d) \quad (1)$$

where T(d) is the total image count and P(d) is the primary (non-scattered) count. Using the theoretical attenuation coefficient μ_a and the primary count P(0) at d = 0, P(d) is represented by

$$P(d) = P(0) \exp(-\mu_a d) \quad (2)$$

From Eqs. (1) and (2), the SF value (= S(d)/P(d)) for a water equivalent material thickness d was calculated. In this study, we considered the counts measured in air as the primary count P(0) and used the theoretical attenuation coefficient μ_a of 0.187 cm $^{-1}$ for water equivalent material.⁵ The P(0) and T(d) were obtained from the ROIs (areas with 1% count-threshold of the maximum image counts) set on the images in air and with forward scattering materials thickness d.

For four cold lesions (1 cm ϕ , 2 cm ϕ , 3 cm ϕ , and 4 cm ϕ)

on the planar images of the Tl-201 plate phantom with multiple defects, the cold lesion contrast value CV was calculated by the following equation:

$$CV = (C_{BG} - C_D)/C_{BG} \quad (3)$$

where C_D was the counts/pixel for an ROI (3 × 3 pixels) in the defects and C_{BG} was the counts/pixel for an ROI (9 × 9 pixels) set on the background near these defects.

B. SPECT imaging

An anthropomorphic torso phantom (Data Spectrum Corp., Hillsborough, NC) with a mediastinum, two lungs, and a spinal cord was used in this study. The myocardial phantom with an anterior defect of 2 cm ϕ and Tl-201 of 29.6 MBq was placed in the mediastinum. SPECT data were acquired with a continuous rotation mode (2.5 min × 8 rotations) 60 views over 360° and in 128 × 128 matrices with a pixel size of 4.3 mm. The radius of rotation was changed automatically as the collimator approached the phantom's surface as closely as possible. After Butterworth filtering (order of 8 and cutoff frequency of 0.28 cycles/pixel) to the projection data, transaxial images were reconstructed by a filtered backprojection with a ramp filter. No attenuation correction was performed. Short-axis images were obtained using these transaxial data.

RESULTS

Energy spectra calculated by our Monte Carlo program are shown in Figure 2. The energy resolution was 12%. The x-rays photopeak, which is composed of four different energy emissions, had a shoulder around 80 keV and a width ranging from 56 to 98 keV. The center-of-mass energy for the x-rays photopeak was 72.524 keV and higher than 71 keV corresponding to the peak. It was found that a small amount of down-scatter from the two gamma rays is included in the x-rays photopeak region.

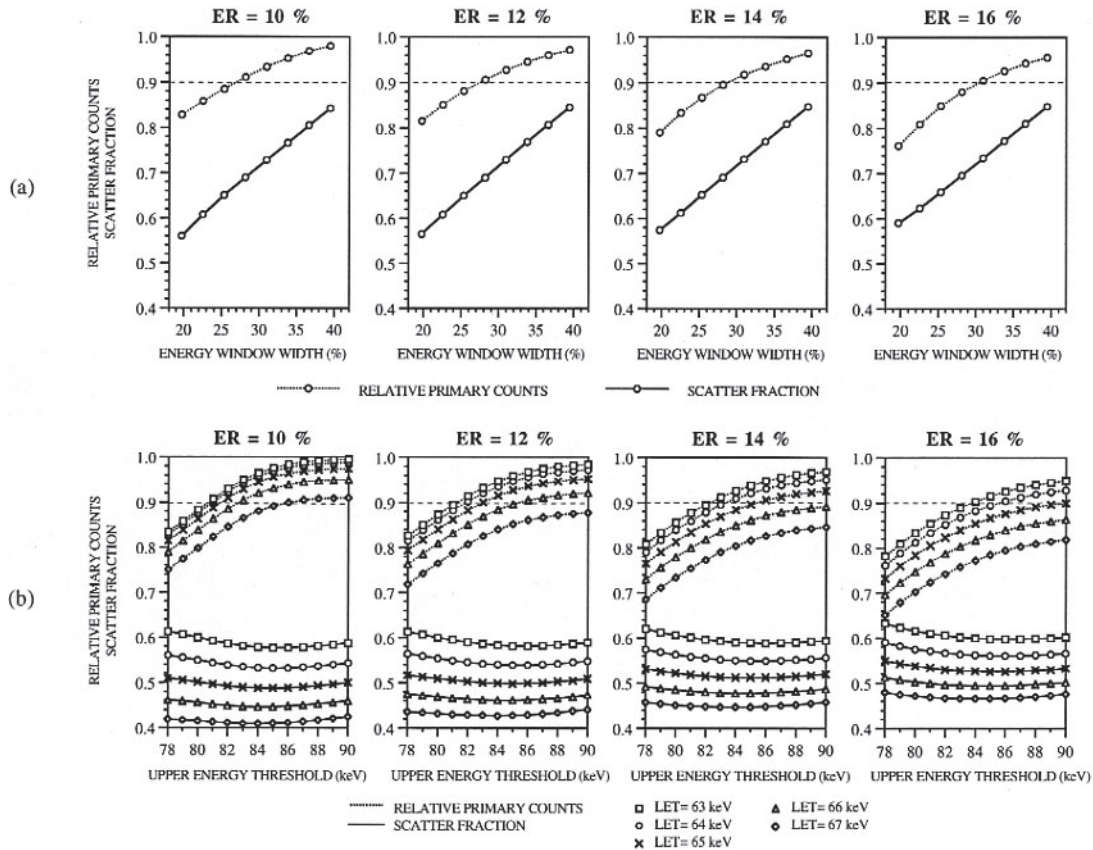


Fig. 3 (a) The relationships between the energy window width (% at 71 keV) and the relative primary counts or the SF for the on-peak window. (b) The relationships between the upper energy threshold (UET) and the relative primary counts or the SF for the off-peak window. The lower energy threshold (LET) was changed from 63 to 67 keV.

Table 1 Optimum off-peak energy window setting for various energy resolutions obtained by the Monte Carlo simulation

Energy resolution at 71 keV	Lower energy threshold (keV)	Upper energy threshold (keV)	Width (keV)	Window setting (center \pm % width)
10%	67	87	20	77 keV \pm 13.0%
12%	66	88	22	77 keV \pm 14.3%
14%	65	87	22	76 keV \pm 14.5%
16%	64	88	24	76 keV \pm 15.8%

The relationships between the energy window width and the relative primary counts or the SF are shown in Figure 3a for the on-peak window and Figure 3b for the off-peak window. As the on-peak window width becomes greater, the primary counts increase according to a saturation curve and the SF value also increases linearly. In this case, since the improvement of the SF value is not dependent on the energy resolution, the better energy resolution does not help to improve the image quality. However, the off-peak window increases primary counts and decreases the SF value (minimum at \sim 86 keV) as the center of window is placed in the higher side from the

peak. Furthermore, the SF value can be made smaller with the lower energy threshold raised and better energy resolution. From these results, the optimum energy window setting for each energy resolution, which can obtain above 90% of the total primary counts and make the SF value as small as possible, is listed in Table 1. For the ER = 12%, the optimum energy window was determined as a wider off-peak window, 77 keV \pm 14.3% (66–88 keV). This off-peak window increased the primary counts rate by 12.5% and decreased the SF by \sim 17% as compared with the conventional on-peak energy window (71 keV \pm 10%, 64–78 keV).

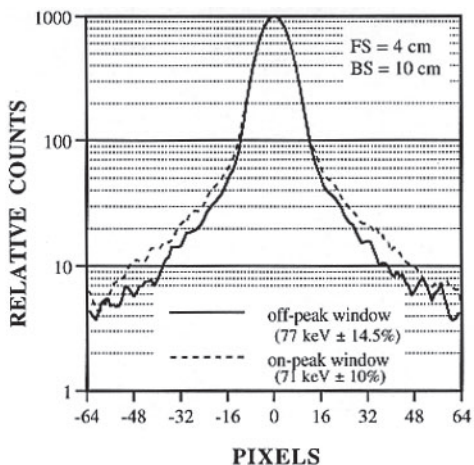


Fig. 4 Tl-201 line source's counts-profile-curves acquired with the off-peak window and the on-peak window. The line source was placed at the 4 cm-forward scatter (FS) and the 10 cm-backscatter (BS) of water-equivalent materials.

Table 2 Comparison of image counts, scatter fraction (SF) value and spatial resolution for planar images of a Tl-201 line source

	Energy window	
	Off-peak window 77 keV ± 14.5%	On-peak window 71 keV ± 10%
Primary counts	71165	64562
Scatter counts	34452	38875
Total counts	105617	103437
SF	0.48	0.60
FWHM (mm)	13.2	13.4
FWTM (mm)	24.8	26.2

Table 3 Comparison of contrast values for four cold lesions in planar images of a Tl-201 plate phantom with multiple defects

Defect size (mm ϕ)	Contrast value	
	Off-peak window 77 keV ± 14.5%	On-peak window 71 keV ± 10%
40	0.79	0.74
30	0.74	0.68
20	0.57	0.52
10	0.27	0.22

Consequently, we applied the off-peak window, 77 keV ± 14.5%, to the phantom imaging by the gamma camera with the ER = 12% and compared it with the on-peak window, 71 keV ± 10%.

Figure 4 illustrates the comparison of counts profile curves obtained from the planar images of the Tl-201 line source within the tough water phantom. The off-peak window had fewer scatter counts than the on-peak window. Table 2 lists the comparison of the image counts, the SF value, FWHM and FWTM. For the primary counts

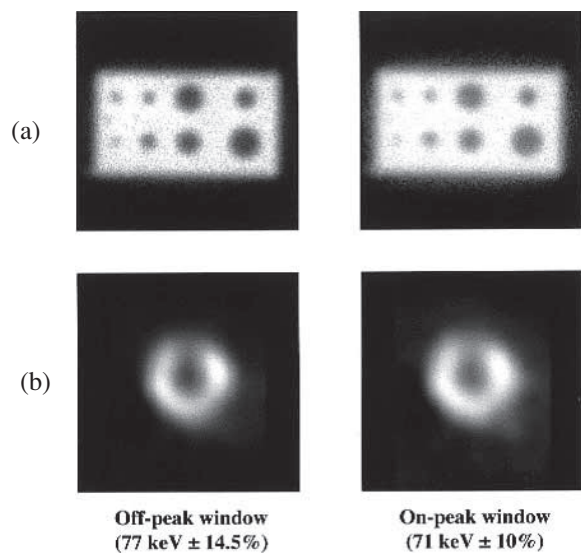


Fig. 5 (a) Planar images of the plate phantom with multiple defects, acquired with the off-peak window and the on-peak window. The total counts (maximum counts) in the image ROI were 2082756 (145) for the off-peak window and 2089914 (137) for the on-peak window. (b) Short axial myocardial phantom SPECT images acquired with the off-peak window and the on-peak window. The total counts (maximum counts) in the image ROI were 89895 (690) for the off-peak window and 85389 (640) for the on-peak window.

obtained by Eq. (2) the off-peak window gave ~10.2% more counts than the on-peak window and this increase rate of primary counts was close to that with the simulation (~12.5%). For the SF value the off-peak window also gave ~20% smaller values than the on-peak window and these measured SF values were also similar to the calculated ones (Fig. 3b); 0.46 for the off-peak window and 0.56 for the on-peak window.

Planar images of the plate phantom with multiple defects and short-axial myocardium SPECT images are shown in Figures 5a and 5b, respectively. As shown in Table 2, since the off-peak window increases the primary counts and decreases the scatter counts within the image ROI as compared with the on-peak window, the total counts with the off-peak window were close to ones with the on-peak window. Improvements in contrast in cold lesions could be seen on the images acquired with the off-peak window. The contrast values measured for the plate phantom were listed in Table 3.

DISCUSSION

The energy resolution of the modern gamma cameras has been improved (<10% at 140 keV) and the shoulder of the Hg-201 x-rays photopeak around 80 keV has been seen on the energy spectrum display.⁵ Conventionally, the energy window centered on the peak of the x-rays photopeak is

employed for Tl-201 imaging, and sometimes the second energy window at 167 keV-gamma ray photopeak is also used. So far, these window settings have been performed empirically. However, setting the center of the energy window on the peak of 71 keV lower than the center-of-mass of 72.524 keV on the x-rays photopeak is equivalent to using an asymmetric energy window moved to the lower half-side of the single energy photopeak.

The simplest technique to reduce scattered photons included the single energy photopeak window without any scatter correction methods is to employ the asymmetric energy window, whose center is moved to the higher energy side than the peak.^{8–11} When this asymmetric energy window is applied to the x-rays photopeak on Tl-201 imaging, we named it “off-peak window” in this study. Changing the symmetric energy window set on the single energy photopeak to the asymmetric energy window has an effect whereby both scattered and primary photons are decreased. However, as shown in Figure 3b, for the asymmetric photopeak of the Hg-201 multiple energy x-rays, although the off-peak window increases scattered photons, it can also increase the more primary photons. Furthermore, the combination of the lower energy threshold and upper energy threshold varies the degree of improvement for both reduction of the SF value and increase of the primary photons. As we reported in Reference,⁷ we determined the energy window setting which can count above 90% of the total primary photons and make the SF value as small as possible to be the optimum off-peak window setting (Table 1). Better energy resolution is an additional advantage. For Tl-201 cardiac imaging, a wider energy window of 30% or 35% whose center is set on the peak is recommended,⁶ but the use of wider off-peak windows of 66–87 keV (76.5 keV–27.5%)¹² or 64–88 keV (76 keV–31.6%),¹³ which were similar to our result, has been also reported in Tl-201 myocardial SPECT imaging.

In this study, we determined the optimum energy window as a wider off-peak window, 77 keV ± 14.3% (66–88 keV) for the ER = 12%, and applied this off-peak window setting (practically, 77 keV ± 14.5%) to planar or SPECT imaging for a plate phantom with multiple cold lesions and an anthropomorphic torso phantom with a myocardium using the gamma camera. When the off-peak widow acquisition was compared with the on-peak window one (71 keV ± 10%), the planar and SPECT images with the off-peak widow clearly showed superior image quality.

The use of the asymmetric or off-peak window causes a problem about a loss of image-uniformity. Planar and SPECT imaging need rigorous uniformity,¹⁴ but the newer full- or semi-digital gamma cameras have a uniformity correction circuit or software to compensate uniformity with flood data. If one wants to acquire scintigraphic images by the off-peak window using the gamma camera without any of these uniformity correction techniques, a

compromise between the effect of the off-peak window and the degree of nonuniformity must be considered. The gamma camera employed in this experiment had the National Electrical Manufacturers Association (NEMA) integral field uniformity of 4.8% at the central field-of-view (CFOV) for the on-peak window. Although that field uniformity became worse up to 6.2% for the off-peak window, no distortion or artifacts were seen on the planar and SPECT images.

Tl-201 also emits gamma rays that have detectable energies (135 and 167 keV) with the gamma camera. Although these gamma rays produce Pb x-rays (~75 keV) from the collimator, the amount of Pb x-rays included within the Hg-201 x-rays photopeak is negligible because of the low abundance of the gamma rays. So we did not consider the Pb x-rays in this investigation. If these gamma rays are collected together with the Hg-201 x-rays, it is expected that the counting rate increases by ~10% and image quality becomes better under the use of a small amount of Tl-201 radioactivity. Now we are investigating improvement of the counting rate (sensitivity) by adding gamma rays window acquisition to the off-peak window one.

In conclusion, the energy window setting of the Hg-201 x-rays for Tl-201 imaging was empirically performed. It is important to decrease the scattered photons relatively or to reduce the SF value while increasing the primary counts rate if no scatter correction methods are employed in scintigraphic imaging. To perform effective Tl-201 imaging, the optimum off-peak window setting was determined for various energy resolutions using the Monte Carlo simulation. As expected from the results of the simulation, in the phantom experiments using the gamma camera with the energy resolution of 12% at 71 keV, effective data acquisition could be achieved with the off-peak window 77 keV ± 14.5% compared with the on-peak window of 71 keV ± 10%.

REFERENCES

1. Beller GA, Bergmann SR. Myocardial perfusion imaging agents: SPECT and PET. *J Nucl Cardiol* 2004; 11: 71–86.
2. Greenspan BS, Brown ML, Dillehay GL, McBiles M, Sandler MP, Seabold JE, et al. Society of Nuclear Medicine procedure guideline for parathyroid scintigraphy, SNM procedure guideline manual. June, 23–27, 2002.
3. Becker DV, Charkes ND, Hurley JR, McDougall IR, Price DC, Royal HD, et al. Society of Nuclear Medicine procedure guideline for extended scintigraphy for differentiated thyroid cancer, SNM procedure guideline manual. June, 19–22, 2002.
4. Browne E, Firestone RB. *Table of radioactive isotopes*. New York; John Wiley & Sons Inc., 1986: 202–202.
5. Kojima A, Matsumoto M, Ohyama Y, Tomiguchi S, Kira M, Takahashi M. Energy spectral analysis in a photopeak region of Hg-201 X-rays for Tl-201 imaging. *KAKUIGAKU (Jpn J Nucl Med)* 1997; 34: 95–103.

6. Depuey EG (ed), Update imaging guidelines for nuclear cardiology procedures part 1. *J Nucl Cardiol* 2001; 8: G5–G10.
7. Kojima A, Matsumoto M, Takahashi M, Uehara S. Effect of energy resolution on scatter fraction in scintigraphic imaging: Monte Carlo study. *Med Phys* 1993; 20: 1107–1113.
8. Rollo FD, Schulz AG. Effect of pulse-height selection on lesion detection performance. *J Nucl Med* 1971; 12: 690–699.
9. Sanders TP, Sanders TD, Kuhl DE. Optimizing the window of an anger camera for Tc-99m. *J Nucl Med* 1971; 12: 703–706.
10. La Fontaine RL, Stein MA, Graham LS, Winter J. Cold lesions: enhanced contrast using asymmetric photopeak windows. *Radiology* 1986; 160: 255–260.
11. Graham LD, La Fontaine RL, Stein MA. Effect of asymmetric photopeak windows on flood field uniformity and spatial resolution of scintillation camera. *J Nucl Med* 1986; 27: 706–713.
12. Chang W, Henkin RE. Photon attenuation in Tl-201 myocardial SPECT and quantitation through an empirical correction. In: Esser PD, ed. *Emission computed tomography: current trends*. New York; The Society of Nuclear Medicine, 1983: 123–133.
13. Kadrmas DJ, Frey EC, Tsui BMW. Simultaneous technetium-99m/thallium-201 SPECT imaging with model-based compensation for cross-contaminating. *Phys Med Biol* 1999; 44: 1843–1860.
14. Rogers WL, Clinthorne NH, Harkness BA, Koral KF, Keyes JW. Field-flood requirement for emission computed tomography with an anger camera. *J Nucl Med* 1982; 23: 162–168.